Polymeric Encapsulation of a Ruthenium Polypyridine Complex for Tumor Targeted One- and Two-Photon Photodynamic Therapy

Johannes Karges, Jia Li, Leli Zeng, Hui Chao, Gilles Gasser

Polymeric Encapsulation of a Ruthenium Polypyridine Complex for Tumor Targeted 1- and 2-Photon Photodynamic Therapy

Johannes Karges[a], Jia Li[b], Leli Zeng[b,c], Hui Chao[b,] and Gilles Gasser[a,]**

[a] Chimie ParisTech, PSL University, CNRS, Institute of Chemistry for Life and Health Sciences, Laboratory for Inorganic Chemical Biology, 75005 Paris, France.

[b] MOE Key Laboratory of Bioinorganic and Synthetic Chemistry, School of Chemistry, Sun Yat-sen University, 510275 Guangzhou, People's Republic of China.

[c] Research Centre, The Seventh Affiliated Hospital, Sun Yat-Sen University, Shenzhen 518107, People's Republic of China.

KEYWORDS

Anticancer, Bioinorganic Chemistry, Medicinal Inorganic Chemistry, Metals in Medicine, Photodynamic Therapy.

ABSTRACT

Photodynamic therapy is a medical technique, which is gaining increasing attention to treat various types of cancer. Among the investigated classes of photosensitizers, the use of Ru(II) polypyridine complexes is gaining momentum. However, the currently investigated compounds generally show poor cancer cell selectivity. As a consequence, high drug doses are needed, which can cause side effects. To overcome this limitation, there is a need for the development of a suitable drug delivery system to increase the amount of PS delivered to the tumor. Herein, we report on the encapsulation of a promising Ru(II) polypyridyl complex into polymeric nanoparticles with terminal biotin groups. Thanks to this design, the particles showed much higher selectivity for cancer cells in comparison to non-cancerous cells in a 2D monolayer and

3D multicellular tumor spheroid model. As a highlight, upon intravenous injection of an identical amount of the Ru(II) polypyridine complex, an improved accumulation inside an adenocarcinomic human alveolar basal epithelial tumor of a mouse by a factor of 8.7 compared to the Ru complex itself was determined. The nanoparticles were found to have a high phototoxic effect upon 1-photon (500 nm) or 2-photon (800 nm) excitation with an eradication of an adenocarcinomic human alveolar basal epithelial tumor inside a mouse. Overall, this work describes, to the best of our knowledge, the first *in vivo* study demonstrating the cancer cell selectivity of a very promising Ru(II)-based PDT photosensitizer encapsulated into polymeric nanoparticles with terminal biotin groups.

INTRODUCTION

The number of patients diagnosed with cancer is steadily increasing. Despite recent improvements in the diagnosis and treatments of this disease, it remains the leading cause for mortality in the developed world. New methods and/or drugs are urgently needed to meet with the challenges associated with the treatment of this disease. As a complementary technique to traditional modality treatments (i.e., chemotherapy, radiotherapy, surgery), increasing attention is currently devoted towards photodynamic therapy (PDT). During a PDT treatment, a photosensitizer (PS) is activated to photo-catalytically generate reactive oxygen species (ROS). As these species are highly reactive, they can rapidly interact with their biological surroundings to cause oxidative damage and ultimately trigger cell death.[1-3] During recent years, the use of transition metal complexes, and especially Ru(II) polypyridine complexes, has gained much attention due to their attractive chemical and photophysical properties (e.g., chemical stability and photostability, high water solubility, high ROS production).[4-14] Despite their remarkable abilities to act as PSs, these compounds have generally a poor cancer cell selectivity. As a consequence, high drug doses are needed, which can cause side effects. While the PS itself should ideally be non-toxic in the dark, it generates cellular damage when exposed to light. Since skin and tissue are strongly scattering the delivered light during the treatment, and since strict irradiation of the tumor site is a practical challenge, the surrounding healthy tissue is typically also damaged. To overcome these drawbacks, there is a need for the development of a drug delivery system, which can selectively transport the Ru-based PS to its target.

To date, different classes of delivery systems have been developed. Typically, these are differentiated between active and passive pathways. During the active targeting of a tumor, a specific interaction of a molecule, such as a signaling peptide, oligonucleotide, oligosaccharide,

protein, receptor targeting moiety or an antibody, is used to transport the therapeutic molecule.[15-17] A large variety of transition metal complexes have been successfully coupled to peptides resulting in increased receptor selectivity.[18-20] As examples for Ru(II) polypyridine complexes, the conjugation to the peptide hormone somatostatin showed a 100-fold increased selectivity for somatostatin receptor-expressing cells relative to the free PS.[21] The covalent conjugation of a Ru(II) polypyridine complex to the human gastrin-releasing peptide receptor or a nuclear localization signal peptide, resulted in a higher uptake of the conjugate in receptor-expressing cells in comparison with the complex itself.[22] The conjugation of the receptor binding peptides Arg-Gly-Asp (RGD) and octreotide, which are overexpressed in various kinds of cancers, to a Ru(II) arene complex were also reported.[23] Capitalizing on these results, a conjugate consisting of a RGD peptide and a Ru(II) polypyridine was recently reported as a selective prodrug.[24] As a different type of delivery system, the conjugation of a Ru(II) polypyridine complex to an epidermal growth factor receptor specific nanobody was shown to have high selectivity for this receptor.[25] Recently the conjugation of a Ru(II) polypyridine to the blood plasma protein serum albumin as a mitochondria selective delivery system was reported.[26] On the contrary, when a passive targeting approach is taken, the nature of the tumour, which includes its leaky, highly permeable vasculature and poor lymphatic tissue characteristics, is used to selectively bring a drug to its target. This passive targeting approach could be achieved by oil dispersions, loading onto nanoparticles, encapsulation in polymeric particles or liposomes[27-29], although this concept is currently controversial discussed.[30] As examples, selenium[31-33], silver[34], gold[35-37] and silicon[38-40] nanoparticles as well as upconverting[41-43] nanoparticles were successfully loaded with Ru(II) polypyridine complexes, forming a drug delivery vehicle. Further, the physical encapsulation of Ru(II) polypyridine complexes into polymeric particles[44-49], micelles[50-52], dendrimers[53] or liposomes[54-55] was reported. Despite these efforts, the majority of the previously mentioned transport systems are associated with a poor water solubility, tedious preparation, high price or a diminished therapeutic effect. To overcome these limitations, there is an urgent need for a simple, water-soluble, cheap and selective delivery system.

In this work, the encapsulation of [Ru((*E*,*E*')-4,4′-bis[*p*-methoxystyryl]-2,2′-bipyridine)(2,2′-bipyridine)$_2$]$^{2+}$ (**Ru**, Figure 1a), an efficient PS for 1-Photon (1P) and 2-Photon (2P) PDT,[56] with 1,2-distearoyl-sn-glycero-3-phosphoethanolamine-*N*-[biotin (poly-ethyleneglycol)-2000] ammonium salt (DSPE-PEG$_{2000}$-biotin, Figure 1b) was envisioned to act as a delivery system for the PS. PEGylated phospholipid polymer was chosen in this work since it is approved by the US Food and Drug Administration for medical applications.[57] The PS **Ru** (Figure 1a) was

selected in this study due to its impressive photophysical/biological properties including the ability to eradicate, *in vivo,* a multi-resistant cancer tumour.[56, 58] Overall, the concept of our work is based on dual tumor selectivity: 1) the polymer carrier can target tumor tissue due to the enhanced permeability and retention (EPR) effect[59-60]; 2) biotin as a member of the vitamin B family is majorly taken up by cells through the sodium multivitamin transporter (SMVT). As this receptor is overexpressed in a variety of cancers, and since there is a high demand for biotin in rapidly growing cells, the encapsulation in a biotin-containing polymer can provide an additional cancer cell targeting effect.[61-62] This hypothesis could be demonstrated in this work with the selective accumulation of the nanoformulation of **Ru** (called **NP** in this work) in 2D monolayer cancer cells and 3D multicellular tumor spheroids. In addition, the tumor targeting effect could be validated with an 8.7 times increased accumulation of **NP** inside an adenocarcinomic human alveolar basal epithelial tumor of a mouse compared to **Ru** using the same concentration of the Ru(II) polypyridine complex. Importantly, upon photoactivation, **NP** was found to kill various types of cancer cells and to eradicate a tumor inside a mouse upon 1P (500 nm) or 2P (800 nm) excitation. To the best of our knowledge, this work describes, the first study demonstrating the *in vivo* cancer cell selectivity of a very promising Ru(II)-based PDT photosensitizer encapsulated into polymeric nanoparticles with terminal biotin groups.

RESULTS AND DISCUSSION

Ru was synthesized as previously reported (Scheme S1).[56] The purity of the compound was confirmed by elemental, NMR (Figure S1) and HPLC analysis (Figure S2). **Ru** was encapsulated with DSPE-PEG_{2000}-biotin, which consists of a lipophilic part (Figure 1b, blue) and hydrophilic part (Figure 1b, green) to form the nanoparticle formulation **NP** (Figure S3). Upon placing this amphiphilic polymer chain in an aqueous phase, the lipophilic parts interact to generate a particle in which core lipophilic compounds could be encapsulated. For a potential cancer targeting effect, biotin groups (Figure 1b, red) were attached to the end of the hydrophilic moiety. After nanoparticle formation, large aggregates were removed by size exclusion chromatography. The amount of encapsulated Ru complex was determined using inductively coupled plasma mass spectrometry (ICP-MS). The isolated nanoparticles have a spherical shape, as indicated by transmission electron microscopy (TEM) imagery (Figure S4). Analysis of the size distribution of **NP** suggested an average size of 94 ± 13 nm by TEM microscopy and 102 ± 9 nm by dynamic light scattering (DLS, Figure S5). Importantly, the particles were found to have high water solubility.

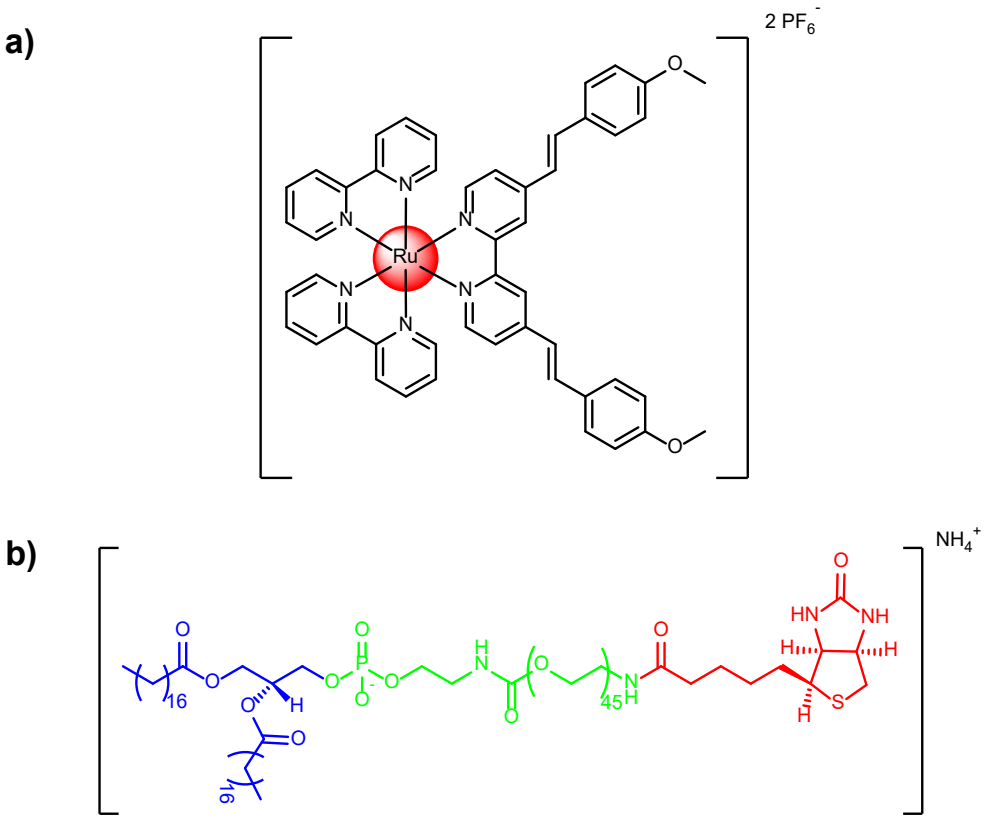

Figure 1. Chemical structures of **a)** the PS [Ru(2,2′-bipyridine)$_2$ ((*E*,*E*')-4,4′-bis[*p*-methoxystyryl]-2,2′-bipyridine)]$^{2+}$ (**Ru**). **b)** the polymer 1,2-distearoyl-sn-glycero-3-phosphoethanolamine-*N*-[biotin (polyethyleneglycol)-2000] [ammonium salt] (DSPE-PEG$_{2000}$-biotin). The hydrophilic (blue) and lipophilic (green) part as well as biotin (red) are marked in color.

The photophysical properties of **Ru** were compared with **NP** to evaluate if the encapsulation changed these properties. As expected, no significant differences in the absorption and emission spectra (Figure S6-S7) were detected. Importantly, the nanoparticles were found to have a higher luminescence quantum yield than the complex alone in H_2O ($\Phi_{em,\,Ru}$ = 0.9%, $\Phi_{em,\,NP}$ = 3.1%). Interestingly, this value is in the same range than the luminescence quantum yield for the complex alone in CH_3CN ($\Phi_{em,\,Ru}$ = 2.8%)[56], indicating that the encapsulation could prevent quenching effects from H_2O. The type of ROS generated was then investigated using electron spin resonance spectroscopy upon incubation with the singlet oxygen ($^1O_2$) scavenger 2,2,6,6-tetramethylpiperidine. While no signal for **NP** was observed in the dark, the characteristic $^1O_2$-induced triplet signal of 2,2,6,6-tetramethylpiperidinyloxyl was observed upon irradiation at 500 nm (Figure S8), confirming the generation of $^1O_2$. This ability was quantitatively evaluated by capturing the highly reactive $^1O_2$ with 1,3-diphenylisobenzofuran and following its temporal production by absorption spectroscopy upon irradiation. Interestingly, the nanoparticles were

found to have a slightly higher singlet oxygen quantum yield than the complex alone ($\Phi(^1O_2)_{Ru}$ = 9%, $\Phi(^1O_2)_{NP}$ = 13%). Overall, these results indicate that the encapsulation improved the photophysical properties in H_2O. Worthy of note, we recently showed that the covalent polymeric encapsulation of a Ru(II) polypyridine complex can improve the photophysical properties in an aqueous solution.[45]

As an important parameter for medical applications, the stability of **NP** was investigated as previous studies have shown that this could be problematic not only for metal complexes but also for nanoparticle formulations. The particles were incubated in H_2O for various time points (0, 1, 4, 12, 24, 48, 72, 96, 168 h) and changes in their absorption spectra (Figure S9) and size distribution determined by DLS (Figure S10) were monitored. No significant differences were observed, indicating the stability of **NP**. Worthy of note, previous investigations for the encapsulation of other metal complexes with the same polymer material have shown that the generated particles were also stable at a reduced pH of 5.[63]

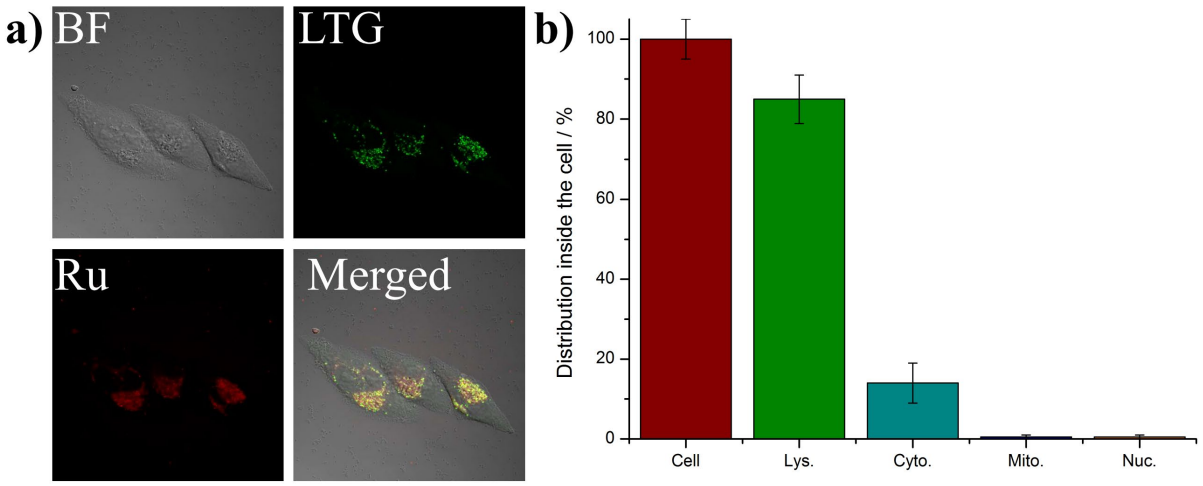

Figure 2. Cellular localization of **NP**. **a)** Confocal luminescence image of adenocarcinomic human alveolar basal epithelial (A549) cells incubated with **NP** (10 µM, λ_{ex} = 458 nm, λ_{em} = 600 - 750 nm) and LysoTracker Green (LTG, 500 nM, λ_{ex} = 488 nm, λ_{em} = 490 - 550 nm) for 4 h at 37°C in the dark. **b)** Subcellular distribution (Cell = whole cell, Lys. = lysosome, Cyto. = cytoplasm, Mito. = mitochondria, Nuc. = nucleus) of **NP** in A549 cells after 4 h incubation in the dark, extraction of their cellular organelles and determination of the amount of Ru inside each organelle by ICP-MS.

The cellular localization of **NP** in adenocarcinomic human alveolar basal epithelial (A549) cells was determined by confocal laser scanning microscopy using the commercially available dyes

for nuclear (Hoechst 33342), mitochondria (MitoTracker Deep Red) and lysosome (LysoTracker Green, LTG) staining. The comparison of the distribution pattern (Figure 2a) indicates a selective colocalization of **NP** in the lysosomes. For quantification of the localization, the major cellular organelles (i.e., nucleus, mitochondria, lysosome, cytoplasm) were separately extracted and the amount of Ru inside determined by ICP-MS. As expected, the majority of the nanoparticles were found inside the lysosomes (Figure 2b) with small amounts in the cytoplasm, confirming the results of the confocal microscopy study. Worthy of note, homoleptic zinc(II) dipyrromethene complexes and large organic aromatic systems, which were encapsulated with the same polymer matrix but with different terminal group were also found mostly in the lysosomes.[63-64]

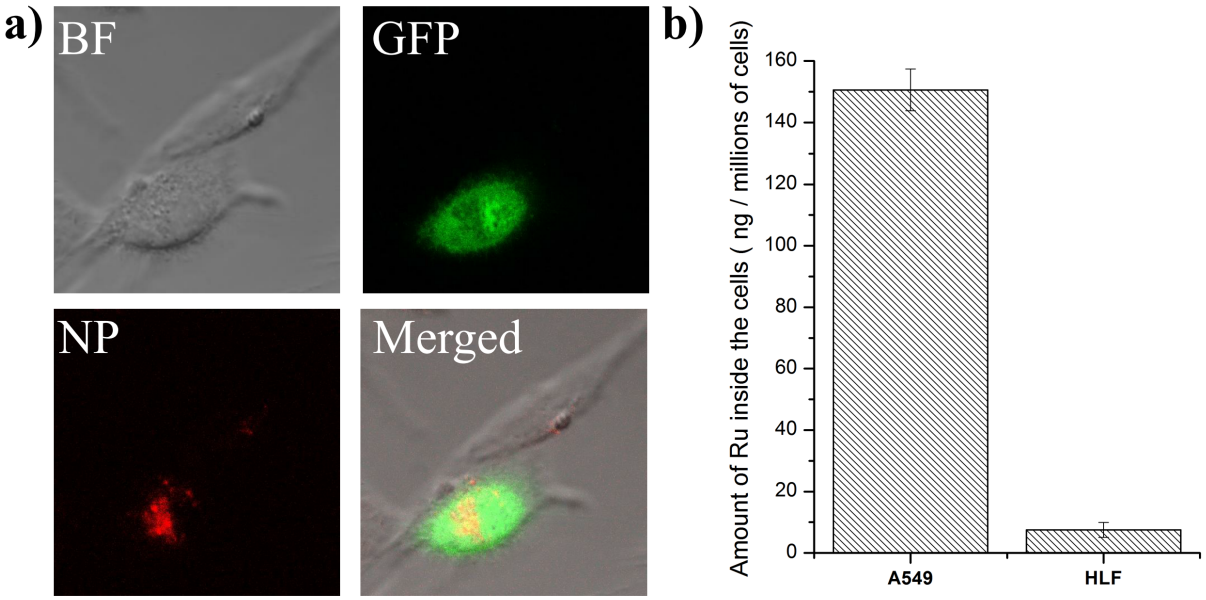

Figure 3. Uptake of **NP** between cancerous adenocarcinomic human alveolar basal epithelial (A549) cells and non-cancerous human lung fibroblasts (HLF) cells. **a)** Confocal luminescence image of a mixture of transfected A549 cells with the green fluorescent protein (λ_{ex}= 458 nm, λ_{em} = 500 - 600 nm) and non-transfected HLF cells incubated for 4 h with **NP** (4.95 µM, λ_{ex} = 514 nm, λ_{em} = 600 - 750 nm) at 37 °C in the dark. **b)** Uptake of **NP** (4.95 µM) after incubation for 4 h at 37 °C in the dark with A549 and HLF cells determined by ICP-MS.

Following this, the cellular uptake mechanism of **NP** in A549 cells was investigated. As there is a higher demand for biotin in rapidly growing cells than in healthy cells, biotin and its conjugates are internalized by the sodium multivitamin transporter (SMVT), which is overexpressed in a variety of cancers.[61-62] Therefore, the terminal conjugation to biotin could provide cancer selectivity. To study the uptake mechanism of **NP**, different internalization

pathways were blocked upon preincubation with metabolic (2-deoxy-D-glucose and oligomycin), cationic transporter (tetraethylammonium chloride), endocytotic (ammonium chloride or chloroquine) and SMVT (pantothenic acid or lipoic acid) inhibitors (Figure S11). As the incubation with tetraethylammonium chloride did not show a significant effect, the internalization by cationic transporters was ruled out. In contrast, the preincubation with metabolic inhibitors and at 4°C lowered the amount of internalized Ru(II) complex. The incubation with ammonium chloride and chloroquine decreased the uptake, suggesting an endocytosis mechanism. Despite these contributions for the internalization of **NP**, the incubation with pantothenic acid or lipoic acid drastically decreased the uptake. This is indicative that the nanoparticles are primarily internalized through a SMVT mediated transportation mechanism. The targeting effect (Figure 3a) was investigated by mixing non-cancerous human lung fibroblasts (HLF) cells with cancerous A549 cells, which were previously transfected to generate the green fluorescent protein (GFP). Worthy of note, these are different cell lines which have intrinsically different properties including uptake, accumulation and toxicity. Using confocal laser scanning microscopy, the red luminescence signal of **NP** could be only detected in the transfected cancerous cells, indicating that the particles selectively accumulated in the cancer cells in comparison to healthy cells. After a qualitative evaluation of the targeting of cancerous cells, this effect was quantified by measuring the amount of internalized Ru by ICP-MS (Figure 3b). Strikingly, **NP** was internalized more than 20 times better in A549 than in HLF cells, confirming the selective accumulation of **NP** in cancer cells.

The ability of **NP** to act as a PS in living cells was then investigated by incubating **NP** with 2′,7′-dichlorofluorescein diacetate (DCFH-DA) in A549 cells, which is converted into the highly fluorescent 2′,7′-dichlorofluorescein (DCF) in the presence of ROS. Promisingly, upon light exposure, a strong green luminescence signal was detected inside the cells (Figure S12), suggesting the production of ROS and therefore the ability of **NP** to act as a PDT agent. Capitalizing on this, the phototoxic effect of **NP** was quantitatively evaluated by determining its cytotoxicity in the dark, upon 1P (500 nm, 11 mW/cm^2, 6.0 J/cm^2) or 2P (800 nm, 0.29 mW/cm^2, 80 MHz, 100 fs, 10.1 J/cm^2) irradiation in human cervical carcinoma (HeLa), HLF, A549 and cisplatin resistant human adenocarcinomic alveolar basal epithelial (A549R) cells (Table S1-S2, Figure S13). **NP** was found to be non-toxic in the dark up to high micromolar concentrations (IC_{50} > 494.7 μM) in all investigated cell lines, which is a crucial requirement for a PDT agent. On the contrary, upon light exposure, **NP** was found to have a high phototoxicity in all cancer cell lines ($IC_{50,\,1P}$ = 3.2 – 3.6 μM, $IC_{50,\,2P}$ = 3.2 – 3.5 μM), allowing

the determination of high phototoxic indices (>139 - >155). The cytotoxicity in cancerous cells was found to be in the same range than the unformulated Ru(II) polypyridine complex.[56] Interestingly, the nanoparticles were also found to be active in cisplatin resistant A549R cells, therefore making them potentially useful for the treatment of resistant cancers. Strikingly, **NP** showed a highly decreased cytotoxicity profile in non-cancerous HLF cells ($IC_{50,\,1P}$ = 48.1 μM, $IC_{50,\,2P}$ = 48.2 μM) in comparison to cancerous cells due to its lower uptake. For a deeper investigation of the PDT effect, the treated cells were stained with calcein AM and propidium iodide to differentiate between living and dead cells (Figure S14). In living cells, the non-fluorescent calcein AM is converted by the ubiquitous intracellular esterases into the highly fluorescent calcein. As dead cells are typically characterized by a damaged membrane integrity, propidium iodide, which is not cell membrane permeable, can enter the cell and intercalate into DNA, inducing a strong red fluorescence. As expected, the cells kept in the dark, treated with **NP** in the dark or purely exposed to the light, showed no cell death. In comparison, the cells treated with **NP** as well as being irradiated were found to be mostly dead, confirming the photodynamic effect. Following this, the cellular death mechanism was investigated. As apoptosis is the predominant mechanism for PDT treatments, its role on the cell death mechanism of **NP** was investigated in A549 cells by measuring the activity of caspase-3/7, which is necessary for an apoptosis-induced cell death. As expected, the caspase-3/7 activity was negligibly influenced upon treatment with **NP** in the dark, similarly to cisplatin, which acts by various apoptotic pathways as recently reported on the same cell line.[65] On the contrary, the caspase-3/7 levels were highly increased upon light irradiation (Figure S15). This indicates that the cell death of **NP** is caused by apoptosis using the caspase-3/7 pathways.

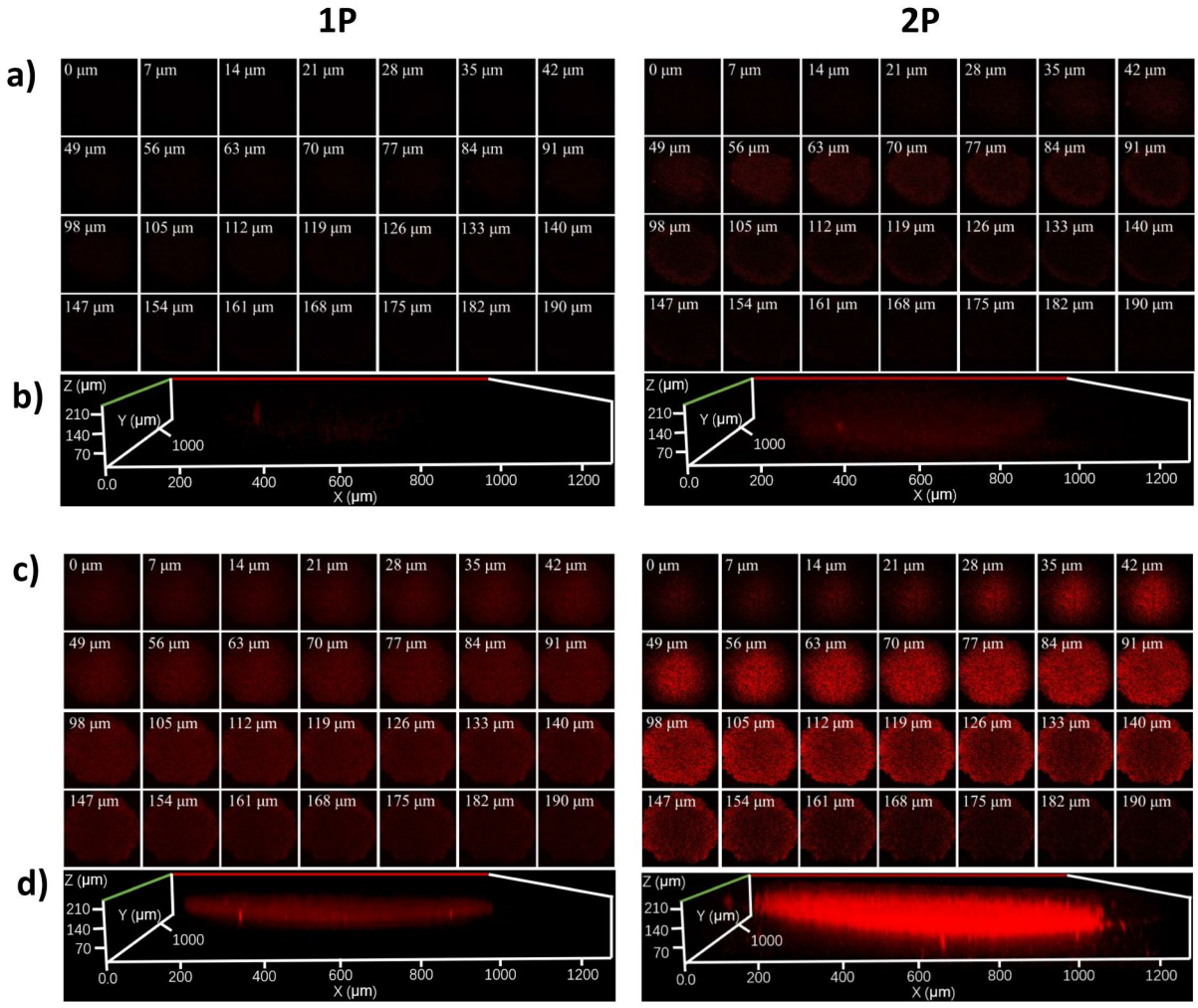

Figure 4. 1P (λ_{ex} = 514 nm, λ_{em} = 600 – 750 nm) and 2P (λ_{ex} = 800 nm, λ_{em} = 600 - 750 nm) excited Z-stack images after incubation of **NP** (4.95 µM) for 12 h in a 500-600 µm noncancerous human lung fibroblasts (HLF) MCTS (**top**) and a 500-600 µm cancerous adenocarcinomic human alveolar basal epithelial (A549) MCTS (**bottom**). **a)/c):** Z-axis images scanning from the top to the bottom of an intact spheroid every 7 µm, **b)/d):** 3D z-stack of an intact spheroid.

After evaluation of the effect of the particles in 2D monolayer cells, the ability of **NP** to act on a 3D multicellular tumor spheroids (MCTS) model was investigated. MCTS are able to better mimic the conditions found in a clinically treated tumors, such as proliferation gradients or a hypoxic center.[66] Worthy of note, many anticancer agents, which have shown promising *in vitro* properties, have failed the translation to *in vivo* models due to compromised drug delivery.[67] As a tissue model, MCTS are able to simulate these conditions and can therefore be used to investigate drug delivery. Capitalizing on this, in this study, the drug delivery of **NP** inside of MCTS with a diameter of 500 - 600 µm was studied by 1P (514 nm) and 2P (800 nm) z-scan

confocal laser scanning microscopy. The nanoparticles showed a bright luminescence signal at every section depth corresponding with a full penetration to the tumor center. Importantly, while only a weak luminescence signal was observed in non-cancerous HLF MCTS, a bright signal was detected in cancerous A549 MCTS (Figure 4). In addition to the previously observed cancer targeting effect in 2D monolayer cells, this observation demonstrates that **NP** is also able to selectively target 3D cancer tumors in comparison to healthy tissue. Following this, the ability of **NP** to act as a PS inside a 3D tissue model was investigated upon incubation with the ROS indicator DCFH-DA inside A549 MCTS. As anticipated, upon treatment in the dark, no significant signal was detected, corresponding with a lack of production of ROS. In comparison, upon exposure to light, a bright green fluorescent signal of DCF was measured (Figure S16), indicating that **NP** is able produce ROS inside a 3D cellular architecture. The dark and photocytotoxicity in A549 MCTS was then quantified by measuring the ATP concentration of living cells and their conversion into chemiluminescence. Importantly, no measurable cytotoxicity in the dark could be observed for **NP** up to high micromolar concentrations (IC_{50} > 494.7 μM). In contrast, **NP** was found to have a high cytotoxicity upon 1P (500 nm, 11 mW/cm^2, 6 J/cm^2) or 2P (800 nm, 0.29 mW/cm^2, 80 MHz, 100 fs, 10.1 J/cm^2) irradiation ($IC_{50,\ 1P}$ = 5.6 ± 0.7 μM, $IC_{50,\ 2P}$ = 4.4 ± 0.6 μM), corresponding to high phototoxic indices of >108.7 or >113.6, respectively. For a deeper understanding of the photodynamic effect, the treated MCTS were stained with calcein AM to investigate if the MCTS are still intact (Figure S17). The MCTS treated with **NP** but kept in the dark showed a bright green fluorescence, indicating that the MCTS consist of living cells. In contrast, the MCTS treated with **NP** and exposed to light had only a negligible fluorescent signal, confirming the death of the 3D MCTS.

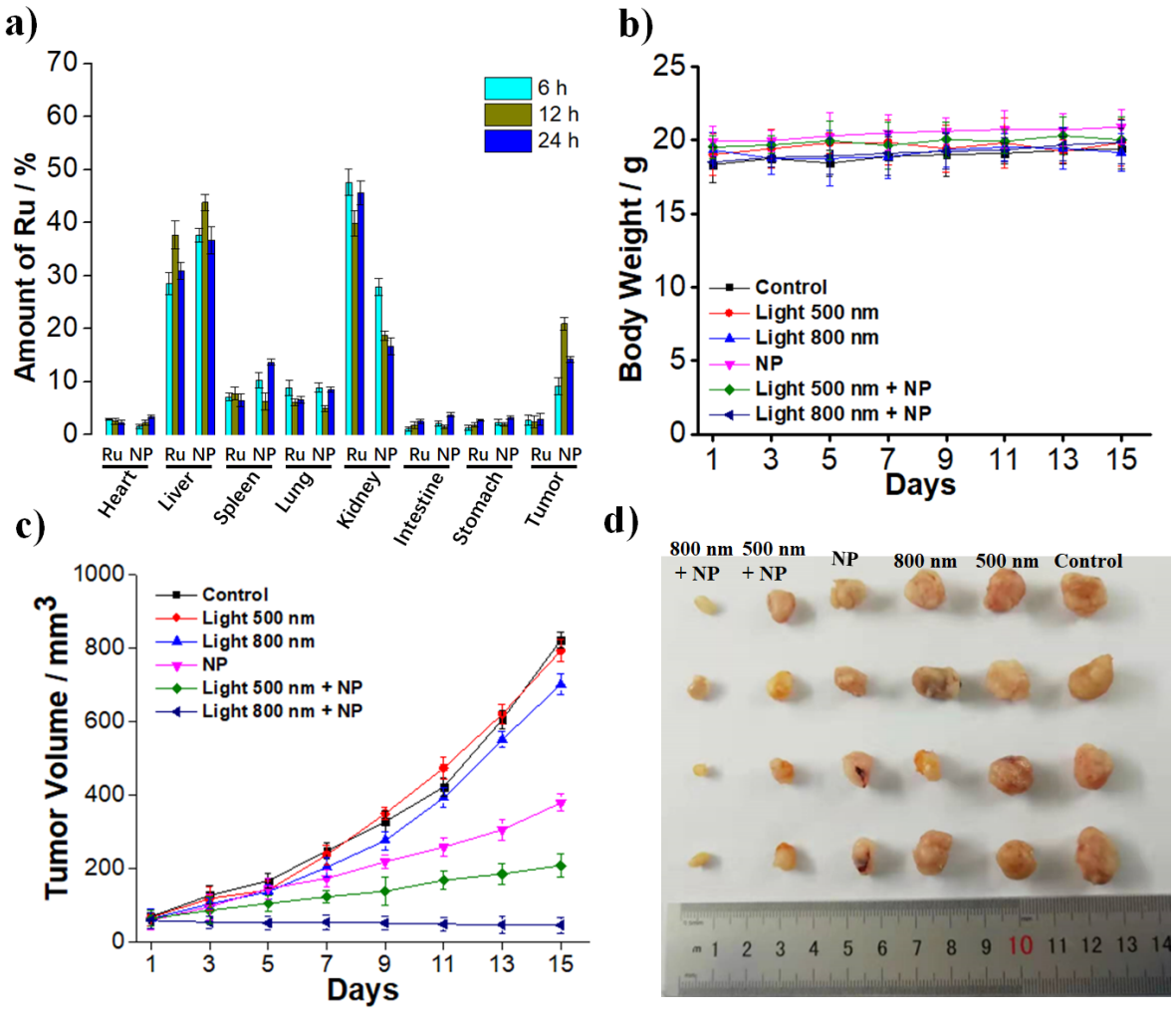

Figure 5. *In Vivo* PDT study of A549 bearing nude mice. **a)** Time dependent biodistribution of **NP** in comparison to **Ru** determined by ICP-MS after 6 h, 12 h, 24 h upon injection of the same amount of the Ru(II) polypyridine complex (3 mg/Kg). **b)** Average body weights of the tumor-bearing mice. **c)** Tumor growth inhibition curves upon 1P (500 nm, 10 mW/cm^2, 60 min) or 2P (800 nm, 50 mW, 1 kHz, pulse width 35 fs, 5 s/mm) treatment. **d)** Representative photographs of tumors harvested 15 days after the treatment.

Based on the promising results obtained from the cellular studies, the ability to act in an *in vivo* nude mouse model bearing A549 tumors was investigated. Previous studies have shown that female nude mice without an intact immune system present a suitable initial model for the ability of anticancer agents.[68] The biodistribution of the formulated **NP** in comparison to the unformulated **Ru** was determined upon intravenous injection of the same amount of the Ru(II) polypyridine complex (3 mg/Kg) in the tail, collection of all major organs (heart, liver, spleen, lung, kidney, intestine, stomach, tumor) followed by determination of the amount of Ru inside by ICP-MS (Figure 5a). The particles showed the highest accumulation within the tumor tissue

after 12 h. Strikingly, **NP** (874 ppb of Ru per 200 mg of tumor tissue) showed an 8.7 times higher accumulation than the unformulated **Ru** (100 ppb of Ru per 200 mg of tumor tissue), demonstrating the *in vivo* tumor accumulation. Importantly, the mice did not lose or gain any weight (Figure 5b) and did not show any signs of stress of discomfort. Following this, mice bearing A549 tumors of 65-70 mm^3 size were treated 12 h after intravenous injection of **NP** with a 1P (500 nm, 10 mW/cm^2, 60 min) or 2P (800 nm, 50 mW, 1 kHz, pulse width 35 fs, 5 s/mm) irradiation. While **NP** itself showed a tumor growth inhibitory effect, the tumor shrank upon 1P irradiation and was nearly completely eradicated upon 2P irradiation (Figure 5c, representative pictures of the tumors after the treatment: 5d). 15 days after the treatment, the mice were sacrificed and all major organs histologically examined. Importantly, no pathological alterations or tissue damage was observed (Figure S18). Overall, this study demonstrates the high potential of **NP** as a cancer targeting PDT agent.

CONCLUSION

In summary, we have designed a drug delivery system for a Ru(II)-based PDT agent against cancer. The metal complex was encapsulated into polymeric nanoparticles with terminal biotin groups. Thanks to this design, the particles were found to have a high selectivity for cancer cells in comparison to non-cancerous cells in a 2D monolayer model as well as 3D multicellular tumor spheroids. In addition, during *in vivo* studies, using the same amount of the Ru(II) polypyridine complex, the particles were found to have an increased accumulation inside the tumor than the complex itself, demonstrating its cancer targeting effect. Upon light exposure at clinically relevant 1-Photon (500 nm) or 2-Photon (800 nm) excitation, the nanoparticles were found to have a high phototoxic effect in 2D monolayer cells and 3D multicellular tumor spheroids as well as to be able to eradicate a tumor inside a mouse model. We strongly believe that the encapsulation method presented in this article for a Ru(II) polypyridyl complex holds great potential for the development of cancer targeted PDT.

EXPERIMENTAL SECTION

Instrumentation and methods

Using a Bruker 400 MHz NMR spectrometer ^{1}H and ^{13}C NMR spectra were measured. The purity of samples was verified by elemental analyses with a Thermo Flash 2000 elemental analyser and HPLC analysis with the following setup: 2 x Agilent G1361 1260 Prep Pump, Agilent G7115A 1260 DAD WR Detector, Agilent Pursuit XRs 5C18 (100Å, C18 5 µm

250 x 4.6 mm) column, Agilent G1364B 1260-FC fraction collector. The solvents (HPLC grade) were millipore water (0.1% TFA, solvent A) and acetonitrile (0.1% TFA, solvent B). Method: 0-3 minutes: isocratic 95% A (5% B); 3- 17 minutes: linear gradient from 95% A (5% B) to 0% A (100% B); 17-23 minutes: isocratic 0% A (100% B). The system was operated with a flow rate of 1 mL/min and the chromatogram detected at 250 nm. The generated particles were characterized by dynamic light scattering (DLS) measurements using an Omni EliteSizer (Brookhaven) and transmission electron microscopy (TEM) images with a JEM-1400 Plus electron microscope (Jeol). The metal content was analyzed by inductively coupled plasma mass spectrometry (ICP-MS) experiments with an iCAP RQ ICP-MS apparatus (Thermo Fisher). Using $RuCl_3$ as a reference, calibration curves were prepared. The polymer 1,2-distearoyl-sn-glycero-3-phosphoethanolamine-*N*-[biotin(polyethylene glycol)-2000] ammonium salt (DSPE-PEG_{2000}-biotin) was purchased from Sigma Aldrich.

Synthesis of Ru

$[Ru(bipy)_2((E,E')$-4,4′-Bis[*p*-(*N*,*N*-methoxy)styryl]-2,2′-bipyridine)$][PF_6]_2$ (**Ru**) was prepared as previously reported.[100] RP-HPLC: R_t = 12.0 min, Elemental analysis calcd for $C_{48}H_{40}F_{12}N_6O_2P_2Ru$ (%): C 51.30, H 3.59, N 7.48; found: C 51.23, H 3.48, N 7.61.

Preparation of nanoparticle formulation NP

5 mg of **Ru** were dissolved in 0.5 mL DCM and then added to an aqueous solution of 10 mg 1,2-distearoyl-sn-glycero-3-phosphoethanolamine-*N*-[biotin(polyethylene glycol)-2000] ammonium salt (DSPE-PEG_{2000}-biotin) in 19.5 mL H_2O. Using a Scientz – II D ultrasonic homogenizer, the prepared emulsion was treated with ultrasonic pulses in a 2 x 10 min method ($t_{sonication}$ = 2 s, Power = 15%, t_{break} = 1 s) while keeping the temperature of the sample at 25 °C. The organic solvent was removed by evaporation at 50 °C. Using size exclusion chromatography, large aggregates were removed from the solution. Following this preparation, a clear transparent solution of **NP** in H_2O was obtained. Using ICP-MS, the amount of encapsulated metal complex was determined as 0.213 mg/mL (Yield: 85%).

Spectroscopic measurements

Using a Lambda 850 UV/VIS spectrometer (PerkinElmer), the absorption of a samples was measured and using a LS 55 fluorescence spectrometer (PerkinElmer) the emission spectra were measured. To determine the luminescence quantum yield (Φ_{em}), samples were prepared in H_2O with an absorbance of 0.1 at 450 nm. The solution was irradiated at 450 nm and the generated

emission measured. The luminescence quantum yields were calculated by comparison with the reference $[Ru(bipy)_3]Cl_2$ in CH_3CN (Φ_{em}=5.9%)[69] and utilization of the following formula:

$$\Phi_{em,\,sample} = \Phi_{em,\,reference} * (F_{reference} / F_{sample}) * (I_{sample} / I_{reference}) * (n_{sample} / n_{reference})^2 \quad (1)$$

$$F = 1 - 10^{-A} \quad (2)$$

Φ_{em} = luminescence quantum yield, F = fraction of light absorbed, I = integrated emission intensities, n = refractive index, A = absorbance of the sample at irradiation wavelength.

Electron spin resonance measurements

Electron spin resonance spectra were measured on a Bruker Model A300 spectrometer at room temperature (20 mW microwave power, 100 G-scan range, and 1 G field modulation). Samples were dissolved in aerated methanol containing 10 mM 2,2,6,6– tetramethylpiperidine (TEMP) as a singlet oxygen scavenger and sucked into capillary tubes by siphon effect in the dark. Using a LED light source centered at 500 nm (11 mW cm^{-2}) the samples were irradiated for 5 min. The electron spin resonance spectra of the samples were measured while keeping it strictly in the dark as well as after exposure to light.

Singlet oxygen measurements

The generation of singlet oxygen $\Phi(^1O_2)$ was quantified by constant monitoring of the change in absorbance of the singlet oxygen scavenger 1,3-diphenylisobenzofuran (DPBF). Samples were prepared containing the desired compound with an absorbance of 0.2 at 500 nm and DPBF (30 μM) in H_2O. The samples were saturated with air and then irradiated at 500 nm over various time intervals. After each time interval, the absorbance of the samples at 411 nm was recorded using a Lambda 850 UV/VIS spectrometer (PerkinElmer). The difference in absorbance (A_0-A) was determined and plotted against the used time intervals. The slope of the linear regression was calculated and correlated with the singlet oxygen quantum yield using the following equation and comparison with the reference $[Ru(bipy)_3]Cl_2$ in H_2O ($\Phi(^1O_2)$=22%)[70]:

$$\Phi(^1O_2)_{sample} = \Phi(^1O_2)_{reference} * (S_{sample} / S_{reference}) * (I_{reference} / I_{sample}) \quad (3)$$

$$I = I_0 * (1 - 10^{-A}) \quad (4)$$

$\Phi(^1O_2)$ = singlet oxygen quantum yield, S = slope of the linear regression of the plot of the areas of the singlet oxygen luminescence peaks against the irradiation intensity, I = absorbance

correction factor, I_0 = light intensity of the irradiation source, A = absorbance of the sample at irradiation wavelength.

Stability in H_2O

Using absorption spectroscopy and dynamic light scattering measurements, the stability of the sample was investigated in H_2O. The compound was dissolved with an absorption of 0.5 at 450 nm and kept in the dark at room temperature. Using a Lambda 850 UV/VIS spectrometer (PerkinElmer), the absorption spectrum from 300-650 nm and using a Omni EliteSizer (Brookhaven) dynamic light scattering apparatus the size distribution was constantly monitored in various time intervals (0, 1, 4, 12, 24, 48, 72, 96, 168 h) and compared.

Cell culture

All cell lines were obtained from the American Type Culture Collection (ATCC). The cell lines human cervical carcinoma (HeLa), human lung fibroblasts (HLF), adenocarcinomic human alveolar basal epithelial (A549) and cisplatin resistant human adenocarcinomic alveolar basal epithelial (A549R) were cultured in DMEM media supplemented with 10% FBS and 1% penicillin/streptomycin. The cisplatin resistance of A549R cis was maintained by cisplatin treatment (1µM) over one week every month. For a cellular assay, the cells were used one week after the end of the treatment in order to avoid interferences in the results. The cells were cultured at 37°C and 5% CO_2. Before an experiment, the cells were passaged three times.

Intracellular distribution by confocal luminescence imaging

Using the luminescence properties of the samples, the localization of the compound was investigated. $1 \cdot 10^4$ cells were allowed to adhere overnight and incubated for 4 h with the sample (10 µM) at 37°C in the dark. The cells were washed three-times with PBS. Following this, the cells were incubated with MitoTracker® Deep Red (MTR, 500 nM), LysoTracker® Green (LTG, 500 nM) and Hoechst 33342 (Hoechst, 5 µg/mL) at 37 °C for 30 min in the dark. The cells were washed three-times with PBS. Using a 63x oil-immersion lens in an LSM 880 (Carl Zeiss) laser scanning confocal microscope with an Argon and a HeNe laser as well as a GaAsP detector, confocal cell images were taken. All organelle trackers LysoTracker® Green (LTG, λ_{ex} = 488 nm, λ_{em} = 490 - 550 nm), MitoTracker® Deep Red (MTR, λ_{ex} = 633 nm, λ_{em} = 650 - 720 nm), and Hoechst 33342 (Hoechst, λ_{ex} = 405 nm, λ_{em} = 410 - 470 nm) were excited and detected as recommended by the supplier. The investigated samples were detected under usage of their luminescence properties (λ_{ex} = 458 nm, λ_{em} = 600 - 750 nm).

Intracellular distribution by ICP-MS

By measuring the Ru content using ICP-MS, the localization of the samples was determined. $10 \cdot 10^6$ cells were incubated with the sample (10 µM) at 37°C for 4 h in the dark. The cells were detached with trypsin, harvested and the number of cells counted. The amount was equally divided into four portions. In the first portion, the nucleus was extracted using a nucleus extraction kit (Sangon Biotech); in the second portion, the mitochondria was extracted using a mitochondria extraction kit (Sangon Biotech) and in the third portion, the lysosome was extracted using a lysosome extraction kit (GenMed Scientific). Using the fourth portion, the cytoplasm was extracted. The cells were detached with trypsin, harvested and centrifuged. The obtained cell pellet was resuspended in lysis buffer and the cells were lysed. The cellular compartments were separated using a vacuum ultracentrifuge (Optima MAX-XP ultracentrifuge, Beckman Coulter) at 200000 g for 150 min at 4 °C. The supernatant solution was divided. Using a 60% HNO_3 solution, each sample was digested for three days and then diluted to 2% HNO_3 in water. The metal content of the sample was determined by ICP-MS and compared with the references. The metal content was then associated with the number of cells.

Cellular uptake mechanism

The cellular uptake was investigated by systematic inhibition of different uptake pathways and determination of the metal content inside the cells by ICP-MS. For each experiment $1 \cdot 10^6$ cells were pretreated with the corresponding inhibitor.

Control: The cells were incubated with the compound (25 µM) for 1 h at 37°C. The cells were washed with PBS, detached with trypsin, harvested, centrifuged and resuspended. The number of cells on each dish was accurately counted. Using a 60% HNO_3 solution, each sample was digested for three days and then diluted to 2% HNO_3 in water. The metal content of the sample was determined by ICP-MS and compared with the references. The metal content was then associated with the number of cells.

Low temperature: The cells were incubated at 4°C for 1 h, followed by an incubation with the compound (25 µM) for 1 h at 4°C. The cells were washed with PBS, detached with trypsin, harvested, centrifuged and resuspended. The number of cells on each dish was accurately counted. Using a 60% HNO_3 solution, each sample was digested for three days and then diluted

to 2% HNO_3 in water. The metal content of the sample was determined by ICP-MS and compared with the references. The metal content was then associated with the number of cells.

Metabolic Inhibition: The cells were incubated with 2-Deoxy-*D*-glucose (50 mM) and oligomycin (5 μM) for 1h. After this time, the cells were washed with PBS and incubated with the compound (25 μM) for 1 h at 37°C. The cells were washed with PBS, detached with trypsin, harvested, centrifuged and resuspended. The number of cells on each dish was accurately counted. Using a 60% HNO_3 solution, each sample was digested for three days and then diluted to 2% HNO_3 in water. The metal content of the sample was determined by ICP-MS and compared with the references. The metal content was then associated with the number of cells.

Endocytic inhibition: The cells were incubated with NH_4Cl (50 mM) or chloroquine (100 μM) for 1h. After this time, the cells were washed with PBS and incubated with the compound (25 μM) for 1 h at 37°C. The cells were washed with PBS, detached with trypsin, harvested, centrifuged and resuspended. The number of cells on each dish was accurately counted. Using a 60% HNO_3 solution, each sample was digested for three days and then diluted to 2% HNO_3 in water. The metal content of the sample was determined by ICP-MS and compared with the references. The metal content was then associated with the number of cells.

Cation transporter inhibition: The cells were incubated with tetraethylammonium chloride (1 mM) for 1h. After this time, the cells were washed with PBS and incubated with the compound (25 μM) for 1 h at 37°C. The cells were washed with PBS, detached with trypsin, harvested, centrifuged and resuspended. The number of cells on each dish was accurately counted. Using a 60% HNO_3 solution, each sample was digested for three days and then diluted to 2% HNO_3 in water. The metal content of the sample was determined by ICP-MS and compared with the references. The metal content was then associated with the number of cells.

Sodium-dependent multivitamin transporter inhibition: The cells were incubated with pantothenic acid (50 μM) or lipoic acid (50 μM) for 1h. After this time, the cells were washed with PBS and incubated with the compound (25 μM) for 1 h at 37°C. The cells were washed with PBS, detached with trypsin, harvested, centrifuged and resuspended. The number of cells on each dish was accurately counted. Using a 60% HNO_3 solution, each sample was digested for three days and then diluted to 2% HNO_3 in water. The metal content of the sample was

determined by ICP-MS and compared with the references. The metal content was then associated with the number of cells.

Transfection assay between cancerous and non-cancerous cells

Using a transfection kit (Beyotime), A549 cells were transfected with the green fluorescent protein (GFP). Cells which were not successfully transfected cells, were removed using the antibiotic G-418. The cancerous, transfected cells were mixed with an equal amount of non-cancerous, non-transfected HLF cells and allowed to adhere overnight. The mixture of cells was incubated with the compound (4.95 μM) at 37 °C for 4 h in the dark. The cells were washed with three-times PBS and confocal images taken using a LSM 880 (Carl Zeiss) laser scanning confocal microscope equipped with a GaAsP detector. Using the luminescence properties of the investigated compound (λ_{ex} = 514 nm, λ_{em} = 600 - 750 nm) and GFP (λ_{ex}= 458 nm, λ_{em} = 500 - 600 nm) these were detected in the cells.

Uptake assay between cancerous and non-cancerous cells by ICP-MS

$1 \cdot 10^6$ cells/mL of A549/HLF cells were seeded in 10 mL of DMEM and allowed to adhere overnight. The cells were incubated with the compound (4.95 μM) in the dark for 4 h. The media was removed and the cells were washed three times with cold PBS and detached with trypsin. The number of cells on each dish was accurately counted. Using a 20% HNO_3 solution and 10% H_2O_2, each sample was digested for two days and then diluted to 2% HNO_3 in water. The metal content of the sample was determined by ICP-MS and compared with the references. The metal content was then associated with the number of cells.

Irradiation induced cellular singlet oxygen generation in monolayer cells

$1 \cdot 10^4$ cells/mL A549 cells were seeded in 10 mL of DMEM and allowed to adhere overnight. The cells were incubated with the compound (4.95 μM) in the dark for 4 h and the media removed. The cells were further incubated with PBS containing DCFH-DA (5.0 μM) for 30 min. The solution was removed, the cells three-times washed and fresh PBS added. Using a LSM 810 (Carl Zeiss) laser scanning confocal microscope, confocal cellular luminescence images (λ_{ex} = 488 nm, λ_{em} = 510 - 550 nm) were recorded. The cells were exposed to a 2-Photon irradiation (800nm, 0.29 mW cm^{-2}, 80 MHz, 100 fs) for 1 min.

(Photo-)cytotoxicity in monolayer cells

$1 \cdot 10^4$ cells were seeded in 96-well plates (100 µL/well) and allowed to adhere overnight. The cells were randomly separated in a dark and light group. In the dark group, the cells were incubated with the compound for 4 h. In the light group, the cells were incubated with the compound for 4 h and then irradiated either by a 1P (500 nm, 11 mW cm^{-2}, 6 J/cm^2) or 2P (800 nm, 0.29 mW cm^{-2}, 80 MHz, 100 fs, 10.1 J/cm^2) irradiation. The cells from both groups were then incubated for an additional 44 h in the dark. To each well 20 µL of MTT solution (5 mg/mL in PBS) was added and incubated at 37 °C for 4 h. The media was removed and 150 µL of DMSO was added to each well. The absorption at 595 nm of each well was measured on an absorption microplate reader.

Live/dead viability/cytotoxicity in monolayer cells

$1 \cdot 10^4$ A549 cells were seeded in 96-well plates (100 µL/well) and allowed to adhere overnight. In the dark group, the cells were pre-incubated with the compound (4.95 µM) for 4 h. In the light group, the cells were pre-incubated with the compound (4.95 µM) for 4 h and then being irradiated at 500 nm by a LED light (500 nm, 11 mW cm^{-2}, light dose = 6 J/cm^2). Both groups were then incubated for 44 h and stained with calcein-AM (λ_{ex} = 490 nm, λ_{em} = 515 nm) and propidium iodide (λ_{ex} = 536 nm, λ_{em} = 617 nm) and their luminescence detected using an Axio Observer Z1 inverted fluorescence microscope (Carl Zeiss).

Caspase-3/7 activation

Using Caspase-Glo-3/7 assay kit (Promega, USA) the caspase-3/7 activity was measured. $1 \cdot 10^4$ A549 cells were seeded in 96-well plates (100 µL/mL). After 24 h, the cells were treated with cisplatin (20 µM) or the compound (2.47 µM and 4.95 µM) and incubated for 4 h at 37 °C. The light treated cells were exposed to irradiation at 500 nm (11 mW/cm^2, 6 J/cm^2). The cells were further incubated for 12 h in the dark. After this time, Caspase-Glo 3/7 reagent (100 µL) was added and incubated for 1 h at room temperature in the dark. The generated chemiluminescence was measured using a microplate reader (infinite M200 PRO, TECAN).

Generation and analysis of 3D multicellular tumor spheroids (MCTS)

Using a high-pressure autoclave, a suspension of 1% agarose in PBS buffer was heated. The hot emulsion was transferred into wells (50 µL per well) of a 96 cell culture well plate. Following this, the plates were exposed to UV irradiation for 4 h. The agarose base was overlayed with $2 \cdot 10^4$ cells/mL of a cell suspension. Within two-three days MCTS were formed

from the cell suspension. The generated MCTS were cultivated and maintained at 37 °C with 5% CO_2 atmosphere in a cell culture incubator. The medium was replaced every two days. The formation, diameter, integrity, and volume of the MCTS was monitored with a LSM 880 (Carl Zeiss) laser scanning confocal microscope. Using a LSM 880 (Carl Zeiss) laser scanning confocal microscope with an Argon or Coherent Chameleon 2-Photon laser and a GaAsP detector, z-stack confocal luminescence images were taken upon incubation of the compound (4.95 μM) for 12 h upon a 1P (λ_{ex} = 514 nm, λ_{em} = 600 - 750 nm) or 2P (λ_{ex} = 800 nm, λ_{em} = 600 - 750 nm) excitation.

Irradiation induced cellular singlet oxygen generation in 3D MCTS

A549 MCTSs were treated with the compound (4.95 μM) for 12 h in the dark, the culture medium was removed and PBS containing DCFH-DA (10.0 mM) was incubated for 30 min. The solution was removed, the cells washed and fresh PBS added. Confocal luminescence images (λ_{ex} = 488 nm, λ_{em} = 510 - 550 nm) were taken with a LSM 810 (Carl Zeiss) laser scanning confocal microscope before and after the irradiation. The cells were exposed to a 2P irradiation (0.29 mW/cm^2, 80 MHz, 100 fs, section interval: 5 μm) at 800 nm for 1 min.

(Photo-)cytotoxicity in 3D MCTS

MCTS were treated with increasing concentrations of **NP** by replacing 50% of the media with drug supplemented media and incubation for 12 h in the dark. After this time, the MCTS were divided in three identical groups. The first group was strictly kept in the dark. The second group was exposed to a 1P irradiation (500 nm, 11 mW cm^{-2}, 6 J/cm^2) and the third group was exposed to a 2P irradiation (800 nm, 0.29 mW/cm^2, 80 MHz, 100 fs, section interval: 5 μm, 10.1 J/cm^2) using a LSM 880 (Carl Zeiss, Germany) laser scanning confocal microscope equipped with a Coherent Chameleon 2P laser. After the irradiation, all groups were incubated additional 36 h. The ATP concertation was measured using a CellTiter-Glo 3D Cell Viability kit (Promega) by measuring the generated chemiluminescence with an infinite M200 PRO (Tecan) plate reader.

Live/dead viability/cytotoxicity in 3D MCTS

In the dark group, A549 MCTS were pre-incubated with the compound (4.95 μM) for 4 h. In the light group, A549 MCTS were pre-incubated with the compound (4.95 μM) for 4 h before being irradiated (800 nm, 0.29 mW cm^{-2}, 80 MHz, 100 fs). Both groups were then incubated for 44 h and stained by Calcein-AM (λ_{ex} = 488 nm, λ_{em} = 510–550 nm) and their luminescence detected using an an Axio Observer Z1 inverted fluorescence microscope (Carl Zeiss).

Animal tumor xenograft models

All animal experiments were carried out on balb/c nude mice (4-6 weeks old, female, ~20 g) and treated in agreement with the principles of laboratory animal care regulations (People's Republic of China). The tumor xenograft models were generated by suspension of A549 cells (1×10^6) in 100 μL PBS and injection into the back of the mice.

***In vivo* biodistribution**

The *in vivo* biodistribution of a compound in A549 tumor bearing nude mice was determined using ICP-MS. The mice were injected in the tail with the sample (3 mg/Kg). After 4 h, 12 h, 24 h the mice were euthanized and their major organs including heart, liver, spleen, lung, kidney, intestine stomach and tumor were collected. Using a 20% HNO_3 solution and 10% H_2O_2, each sample was digested for two days and then diluted to 2% HNO_3 in water. The metal content of the sample was determined by ICP-MS and compared with the references.

***In vivo* (Photo-)cytotoxicity**

When the tumor size reached about 65-70 mm^3, the tumor-bearing mice (4 mice per group) were randomly divided into six groups and tail injected.

Group 1: injected with the compound (4 mg/Kg 50 μL) intravenously and treated with 800 nm laser (50 mW, 1 kHz, pulse width 35 fs, 5 s/mm) 12 h after injection;

Group 2: injected with the compound (4 mg/Kg 50 μL) intravenously and treated with 500 nm light (10 mW/cm^2, 60 min) 12 h after injection;

Group 3: injected by physiological saline (50 μL) intravenously and treated with 800 nm laser (50 mW, 1 kHz, pulse width 35 fs, 5 s/mm) 12 h after injection;

Group 4: injected by physiological saline (50 μL) intravenously and treated with 500 nm light (10 mW/cm^2, 60 min) 12 h after injection;

Group 5: injected with the compound (4 mg/Kg 50 μL) intravenously;

Group 6: injected with physiological saline (50 μL) intravenously.

The mice were anesthetized by injection of 4% chloral hydrate aqueous solution (0.2 mL/20g). The tumor volume and body weight was measured and recorded every two days. The tumor volume was calculated using the following formula:

$$Volume = \frac{Length \times Width^2}{2} \quad (5)$$

Histological examination

The mice were euthanized and the tumor as well as all major organs were collected and fixated by 4% paraformaldehyde. The samples were stained with hematoxylin and eosin (H&E). Using a Carl Zeiss Axio Imager Z2 microscope, the histological examination was performed.

ACKNOWLEDGMENT

This work was financially supported by an ERC Consolidator Grant PhotoMedMet to G.G. (GA 681679) and has received support under the program "Investissements d' Avenir" launched by the French Government and implemented by the ANR with the reference ANR-10-IDEX-0001-02 PSL (G.G.), the National Science Foundation of China (Nos. 21525105 and 21778079 for H.C.) and the 973 Program (No. 2015CB856301 for H.C.).

AUTHOR INFORMATION

Authors

Johannes Karges - Chimie ParisTech, PSL University, CNRS, Institute of Chemistry for Life and Health Sciences, Laboratory for Inorganic Chemical Biology, 75005 Paris, France.

Jia Li - MOE Key Laboratory of Bioinorganic and Synthetic Chemistry, School of Chemistry, Sun Yat-sen University, 510275 Guangzhou, People's Republic of China.

Leli Zeng - MOE Key Laboratory of Bioinorganic and Synthetic Chemistry, School of Chemistry, Sun Yat-sen University, 510275 Guangzhou, People's Republic of China, Research Centre, The Seventh Affiliated Hospital, Sun Yat-Sen University, Shenzhen 518107, People's Republic of China.

Corresponding Authors

Hui Chao - MOE Key Laboratory of Bioinorganic and Synthetic Chemistry, School of Chemistry, Sun Yat-sen University, 510275 Guangzhou, People's Republic of China, Email: ceschh@mail.sysu.edu.cn, Tel. +86 20 84110613.

Gilles Gasser - Chimie ParisTech, PSL University, CNRS, Institute of Chemistry for Life and Health Sciences, Laboratory for Inorganic Chemical Biology, 75005 Paris, France, Email: gilles.gasser@chimieparistech.psl.eu; Tel. +33 1 44 27 56 02; WWW: www.gassergroup.com.

ORCID-ID

Johannes Karges: 0000-0001-5258-0260
Leli Zeng: 0000-0002-3378-5241
Hui Chao: 0000-0003-4153-5303
Gilles Gasser: 0000-0002-4244-5097

Author Contributions

J.K and J. L. have contributed equally to this work. All authors were involved with the design and interpretation of experiments and with the writing of the manuscript. Chemical and photophysical experiments were carried out by J.K. Cellular biological experiments were carried out by J.K and J. L. Animal testing was carried out by J. L. and L. Z. The work was supervised by H. C. and G. G. All authors have given approval to the final version of the manuscript.

ETHICS APPROVAL

All animal experiments were conducted in compliance with the ethical regulations for animal testing and received approval of the experimental animal managing committee of Sun Yat Sen University.

COMPETING INTERESTS

The authors declare no competing interests.

ASSOCIATED CONTENT

Supporting Information

The Supporting Information is available free of charge at https://pubs.acs.org/doi/XXX

Synthesis of **Ru**; ^{1}H NMR spectrum of **Ru**; HPLC chromatogram of **Ru**; Image of diluted **NP** in water; Transmission electron microscopy image of **NP;** Size distribution determined by dynamic light scattering of **NP;** Absorption spectra of **Ru** and **NP** in H_2O; Emission spectra of **Ru** and **NP** in H_2O; ESR signal of **NP** trapped by TEMP; Temporal changes of the absorption spectra of **NP** upon incubation in H_2O; Temporal changes of the average size of **NP** determined by DLS upon incubation in H_2O; Cell uptake mechanism study of **NP** in the presence of different inhibitors/conditions; Confocal fluorescent images of A549 cells incubated with DCFH-DA and **NP** before and after irradiation; IC_{50} values in the dark and upon 1P irradiation of **NP** in HeLa, HLF, A549 and A549R cells; IC_{50} values in the dark and upon 2P irradiation of **NP** in HeLa, HLF, A549 and A549R cells; Drug response curves under light or dark conditions; Inverted fluorescence microscopy images of a cell live/dead assay of A549 cells upon treatment with **NP** in the dark or exposed to an irradiation; Caspase 3/7 activity in A549 cells treated with **NP** in the dark or upon irradiation; Confocal fluorescent images of A549 MCTS incubated with DCFH-DA and **NP** before and after irradiation; Representative images of A549 MCTS treated with **NP** in the dark or exposed to irradiation and afterwards stained with Calcein AM; Representative pictures of histological examination of the mice organs with H&E stained slices.

REFERENCES

1. McFarland, S. A.; Mandel, A.; Dumoulin-White, R.; Gasser, G., Metal-based Photosensitizers for Photodynamic Therapy: The Future of Multimodal Oncology? *Curr. Opin. Chem. Biol.* **2020,** *56*, 23-27.
2. Heinemann, F.; Karges, J.; Gasser, G., Critical Overview of the Use of Ru(II) Polypyridyl Complexes as Photosensitizers in One-Photon and Two-Photon Photodynamic Therapy. *Acc. Chem. Res.* **2017,** *50* (11), 2727-2736.
3. Karges, J., Combining Inorganic Chemistry and Biology: The Underestimated Potential of Metal Complexes in Medicine. *ChemBioChem* **2020,** accepted, doi: 10.1002/cbic.202000397.
4. Shum, J.; Leung, P. K.-K.; Lo, K. K.-W., Luminescent Ruthenium(II) Polypyridine Complexes for a Wide Variety of Biomolecular and Cellular Applications. *Inorg. Chem.* **2019,** *58* (4), 2231-2247.
5. Karges, J.; Blacque, O.; Goldner, P.; Chao, H.; Gasser, G., Towards Long Wavelength Absorbing Photodynamic Therapy Photosensitizers via the Extension of a $[Ru(bipy)_3]^{2+}$ Core. *Eur. J. Inorg. Chem.* **2019,** *2019* (32), 3704-3712.
6. Lincoln, R.; Kohler, L.; Monro, S.; Yin, H.; Stephenson, M.; Zong, R.; Chouai, A.; Dorsey, C.; Hennigar, R.; Thummel, R. P.; McFarland, S. A., Exploitation of Long-Lived 3IL Excited States for Metal–Organic Photodynamic Therapy: Verification in a Metastatic Melanoma Model. *J. Am. Chem. Soc.* **2013,** *135* (45), 17161-17175.

7. Karges, J.; Heinemann, F.; Jakubaszek, M.; Maschietto, F.; Subecz, C.; Dotou, M.; Vinck, R.; Blacque, O.; Tharaud, M.; Goud, B.; Viñuelas Zahínos, E.; Spingler, B.; Ciofini, I.; Gasser, G., Rationally Designed Long-Wavelength Absorbing Ru(II) Polypyridyl Complexes as Photosensitizers for Photodynamic Therapy. *J. Am. Chem. Soc.* **2020,** *142* (14), 6578-6587.
8. Monro, S.; Colón, K. L.; Yin, H.; Roque, J.; Konda, P.; Gujar, S.; Thummel, R. P.; Lilge, L.; Cameron, C. G.; McFarland, S. A., Transition Metal Complexes and Photodynamic Therapy from a Tumor-Centered Approach: Challenges, Opportunities, and Highlights from the Development of TLD1433. *Chem. Rev.* **2019,** *119* (2), 797-828.
9. Felder, P. S.; Keller, S.; Gasser, G., Polymetallic Complexes for Applications as Photosensitisers in Anticancer Photodynamic Therapy. *Adv. Ther.* **2020,** *3* (1), 1900139.
10. Karges, J.; Heinemann, F.; Maschietto, F.; Patra, M.; Blacque, O.; Ciofini, I.; Spingler, B.; Gasser, G., A Ru(II) Polypyridyl Complex bearing Aldehyde Functions as a Versatile Synthetic Precursor for Long-Wavelength Absorbing Photodynamic Therapy Photosensitizers. *Bioorg. Med. Chem.* **2019,** *27* (12), 2666-2675.
11. Karges, J.; Blacque, O.; Jakubaszek, M.; Goud, B.; Goldner, P.; Gasser, G., Systematic Investigation of the Antiproliferative Activity of a series of Ruthenium Terpyridine Complexes. *J. Inorg. Biochem.* **2019,** *198*, 110752.
12. Karges, J.; Kuang, S.; Ong, Y. C.; Chao, H.; Gasser, G., 1- and 2-Photon Phototherapeutic Effects of Ru(II) Polypyridine Complexes in the Hypoxic Centre of Large Multicellular Tumour Spheroids and Tumour-Bearing Mice. *Chem. Eur. J.* **2020**, accepted, doi: 10.1002/chem.202003486.
13. Dickerson, M.; Sun, Y.; Howerton, B.; Glazer, E. C., Modifying Charge and Hydrophilicity of Simple Ru(II) Polypyridyl Complexes Radically Alters Biological Activities: Old Complexes, Surprising New Tricks. *Inorg. Chem.* **2014,** *53* (19), 10370-10377.
14. Karges, J.; Yempala, T.; Tharaud, M.; Gibson, D.; Gasser, G., A Multi-action and Multi-target RuII–PtIV Conjugate Combining Cancer-Activated Chemotherapy and Photodynamic Therapy to Overcome Drug Resistant Cancers. *Angew. Chem. Int. Ed.* **2020,** *59* (18), 7069-7075.
15. Xiang, H.-J.; Deng, Q.; An, L.; Guo, M.; Yang, S.-P.; Liu, J.-G., Tumor Cell Specific and Lysosome-Targeted Delivery of Nitric Oxide for Enhanced Photodynamic Therapy triggered by 808 nm Near-Infrared Light. *Chem. Commun.* **2016,** *52* (1), 148-151.
16. Jakubaszek, M.; Rossier, J.; Karges, J.; Delasoie, J.; Goud, B.; Gasser, G.; Zobi, F., Evaluation of the Potential of Cobalamin Derivatives Bearing Ru(II) Polypyridyl Complexes as Photosensitizers for Photodynamic Therapy. *Helv. Chim. Acta* **2019,** *102* (7), e1900104.
17. Arora, K.; Herroon, M.; Al-Afyouni, M. H.; Toupin, N. P.; Rohrabaugh, T. N.; Loftus, L. M.; Podgorski, I.; Turro, C.; Kodanko, J. J., Catch and Release Photosensitizers: Combining Dual-Action Ruthenium Complexes with Protease Inactivation for Targeting Invasive Cancers. *J. Am. Chem. Soc.* **2018,** *140* (43), 14367-14380.
18. Zamora, A.; Gandioso, A.; Massaguer, A.; Buenestado, S.; Calvis, C.; Hernández, J. L.; Mitjans, F.; Rodríguez, V.; Ruiz, J.; Marchán, V., Toward Angiogenesis Inhibitors Based on the Conjugation of Organometallic Platinum(II) Complexes to RGD Peptides. *ChemMedChem* **2018,** *13* (17), 1755-1762.

19. Novohradsky, V.; Zamora, A.; Gandioso, A.; Brabec, V.; Ruiz, J.; Marchán, V., Somatostatin Receptor-Targeted Organometallic Iridium(iii) Complexes as novel Theranostic Agents. *Chem. Commun.* **2017,** *53* (40), 5523-5526.
20. Barragán, F.; Carrion-Salip, D.; Gómez-Pinto, I.; González-Cantó, A.; Sadler, P. J.; de Llorens, R.; Moreno, V.; González, C.; Massaguer, A.; Marchán, V., Somatostatin Subtype-2 Receptor-Targeted Metal-Based Anticancer Complexes. *Bioconjugate Chem.* **2012,** *23* (9), 1838-1855.
21. Wang, T.; Zabarska, N.; Wu, Y.; Lamla, M.; Fischer, S.; Monczak, K.; Ng, D. Y. W.; Rau, S.; Weil, T., Receptor Selective Ruthenium-Somatostatin Photosensitizer for Cancer Targeted Photodynamic Applications. *Chem. Commun.* **2015,** *51* (63), 12552-12555.
22. Mari, C.; Pierroz, V.; Leonidova, A.; Ferrari, S.; Gasser, G., Towards Selective Light-Activated RuII-Based Prodrug Candidates. *Eur. J. Inorg. Chem.* **2015,** *2015* (23), 3879-3891.
23. Barragán, F.; López-Senín, P.; Salassa, L.; Betanzos-Lara, S.; Habtemariam, A.; Moreno, V.; Sadler, P. J.; Marchán, V., Photocontrolled DNA Binding of a Receptor-Targeted Organometallic Ruthenium(II) Complex. *J. Am. Chem. Soc.* **2011,** *133* (35), 14098-14108.
24. Zhao, Z.; Zhang, X.; Li, C.-e.; Chen, T., Designing Luminescent Ruthenium Prodrug for Precise Cancer Therapy and Rapid Clinical Diagnosis. *Biomaterials* **2019,** *192*, 579-589.
25. Karges, J.; Jakubaszek, M.; Mari, C.; Zarschler, K.; Goud, B.; Stephan, H.; Gasser, G., Synthesis and Characterization of an Epidermal Growth Factor Receptor-Selective RuII Polypyridyl–Nanobody Conjugate as a Photosensitizer for Photodynamic Therapy. *ChemBioChem* **2020,** *21* (4), 531-542.
26. Chakrabortty, S.; Agrawalla, B. K.; Stumper, A.; Vegi, N. M.; Fischer, S.; Reichardt, C.; Kögler, M.; Dietzek, B.; Feuring-Buske, M.; Buske, C.; Rau, S.; Weil, T., Mitochondria Targeted Protein-Ruthenium Photosensitizer for Efficient Photodynamic Applications. *J. Am. Chem. Soc.* **2017,** *139* (6), 2512-2519.
27. Kim, J.; Yoon, H.-J.; Kim, S.; Wang, K.; Ishii, T.; Kim, Y.-R.; Jang, W.-D., Polymer–metal complex Micelles for the Combination of Sustained Drug Releasing and Photodynamic Therapy. *J. Mater. Chem.* **2009,** *19* (26), 4627-4631.
28. Hong, E. J.; Choi, D. G.; Shim, M. S., Targeted and Effective Photodynamic Therapy for Cancer using Functionalized Nanomaterials. *Acta Pharm. Sin. B* **2016,** *6* (4), 297-307.
29. Kim, C.; Kim, S.-Y.; Lim, Y. T.; Lee, T. S., Synthesis of Conjugated Polymer Nanoparticles with Core-Shell Structure for Cell Imaging and Photodynamic Cancer Therapy. *Macromol. Res.* **2017,** *25* (6), 572-577.
30. Danhier, F., To Exploit the Tumor Microenvironment: Since the EPR Effect Fails in the Clinic, What is the Future of Nanomedicine? *J. Controlled Release* **2016,** *244*, 108-121.
31. Sun, D.; Liu, Y.; Yu, Q.; Zhou, Y.; Zhang, R.; Chen, X.; Hong, A.; Liu, J., The Effects of Luminescent Ruthenium(II) Polypyridyl Functionalized Selenium Nanoparticles on bFGF-induced Angiogenesis and AKT/ERK Signaling. *Biomaterials* **2013,** *34* (1), 171-180.
32. Liu, T.; Zeng, L.; Jiang, W.; Fu, Y.; Zheng, W.; Chen, T., Rational design of Cancer-Targeted Selenium Nanoparticles to antagonize Multidrug Resistance in Cancer Cells. *Nanomedicine* **2015,** *11* (4), 947-958.
33. Sun, D.; Liu, Y.; Yu, Q.; Qin, X.; Yang, L.; Zhou, Y.; Chen, L.; Liu, J., Inhibition of Tumor Growth and Vasculature and Fluorescence Imaging using Functionalized

Ruthenium-Thiol protected Selenium Nanoparticles. *Biomaterials* **2014,** *35* (5), 1572-1583.
34. Wumaier, M.; Yao, T.-M.; Hu, X.-C.; Hu, Z.-A.; Shi, S., Luminescent Ru(ii)-Thiol modified Silver Nanoparticles for Lysosome Targeted Theranostics. *Dalton Trans.* **2019,** *48* (28), 10393-10397.
35. Zhang, P.; Wang, J.; Huang, H.; Chen, H.; Guan, R.; Chen, Y.; Ji, L.; Chao, H., RuNH2@AuNPs as Two-Photon Luminescent Probes for Thiols in Living Cells and Tissues. *Biomaterials* **2014,** *35* (32), 9003-9011.
36. Elmes, R. B. P.; Orange, K. N.; Cloonan, S. M.; Williams, D. C.; Gunnlaugsson, T., Luminescent Ruthenium(II) Polypyridyl Functionalized Gold Nanoparticles; Their DNA Binding Abilities and Application As Cellular Imaging Agents. *J. Am. Chem. Soc.* **2011,** *133* (40), 15862-15865.
37. Rogers, N. J.; Claire, S.; Harris, R. M.; Farabi, S.; Zikeli, G.; Styles, I. B.; Hodges, N. J.; Pikramenou, Z., High Coating of Ru(ii) Complexes on Gold Nanoparticles for Single Particle Luminescence Imaging in Cells. *Chem. Commun.* **2014,** *50* (5), 617-619.
38. Frasconi, M.; Liu, Z.; Lei, J.; Wu, Y.; Strekalova, E.; Malin, D.; Ambrogio, M. W.; Chen, X.; Botros, Y. Y.; Cryns, V. L.; Sauvage, J.-P.; Stoddart, J. F., Photoexpulsion of Surface-Grafted Ruthenium Complexes and Subsequent Release of Cytotoxic Cargos to Cancer Cells from Mesoporous Silica Nanoparticles. *J. Am. Chem. Soc.* **2013,** *135* (31), 11603-11613.
39. Ellahioui, Y.; Patra, M.; Mari, C.; Kaabi, R.; Karges, J.; Gasser, G.; Gómez-Ruiz, S., Mesoporous Silica Nanoparticles Functionalised with a Photoactive Ruthenium(ii) Complex: Exploring the Formulation of a Metal-based Photodynamic Therapy Photosensitiser. *Dalton Trans.* **2019,** *48* (18), 5940-5951.
40. He, L.; Huang, Y.; Zhu, H.; Pang, G.; Zheng, W.; Wong, Y.-S.; Chen, T., Cancer-Targeted Monodisperse Mesoporous Silica Nanoparticles as Carrier of Ruthenium Polypyridyl Complexes to Enhance Theranostic Effects. *Adv. Funct. Mater.* **2014,** *24* (19), 2754-2763.
41. Shi, H.; Fang, T.; Tian, Y.; Huang, H.; Liu, Y., A Dual-Fluorescent Nano-Carrier for Delivering Photoactive Ruthenium Polypyridyl Complexes. *J. Mater. Chem. B* **2016,** *4* (27), 4746-4753.
42. Chen, Y.; Jiang, G.; Zhou, Q.; Zhang, Y.; Li, K.; Zheng, Y.; Zhang, B.; Wang, X., An Upconversion Nanoparticle/Ru(ii) Polypyridyl Complex assembly for NIR-Activated Release of a DNA Covalent-Binding Agent. *RSC Adv.* **2016,** *6* (28), 23804-23808.
43. Meijer, M. S.; Natile, M. M.; Bonnet, S., 796 nm Activation of a Photocleavable Ruthenium(II) Complex Conjugated to an Upconverting Nanoparticle through Two Phosphonate Groups. *Inorg. Chem.* **2020**, accepted, doi: 10.1021/acs.inorgchem.0c00043.
44. Bœuf, G.; Roullin, G. V.; Moreau, J.; Van Gulick, L.; Zambrano Pineda, N.; Terryn, C.; Ploton, D.; Andry, M. C.; Chuburu, F.; Dukic, S.; Molinari, M.; Lemercier, G., Encapsulated Ruthenium(II) Complexes in Biocompatible Poly(d,l-lactide-co-glycolide) Nanoparticles for Application in Photodynamic Therapy. *ChemPlusChem* **2014,** *79* (1), 171-180.
45. Soliman, N.; McKenzie, L. K.; Karges, J.; Bertrand, E.; Tharaud, M.; Jakubaszek, M.; Guérineau, V.; Goud, B.; Hollenstein, M.; Gasser, G.; Thomas, C. M., Ruthenium-Initiated Polymerization of Lactide: A Route to Remarkable Cellular Uptake for Photodynamic Therapy of Cancer. *Chem. Sci.* **2020,** *11* (10), 2657-2663.
46. Soliman, N.; Gasser, G.; Thomas, C. M., Incorporation of Ru(II) Polypyridyl Complexes into Nanomaterials for Cancer Therapy and Diagnosis. *Adv. Mat.* **2020**, accepted, doi: 10.1002/adma202003294.

47. Sun, W.; Li, S.; Häupler, B.; Liu, J.; Jin, S.; Steffen, W.; Schubert, U. S.; Butt, H.-J.; Liang, X.-J.; Wu, S., An Amphiphilic Ruthenium Polymetallodrug for Combined Photodynamic Therapy and Photochemotherapy In Vivo. *Adv. Mater.* **2017,** *29* (6), 1603702.
48. Karges, J.; Chao, H.; Gasser, G., Synthesis, Characterisation and Biological Evaluation of the Polymeric Encapsulation of a Ru(II) Polypyridine Complex with Pluronic F-127/Poloxamer-407 for Photodynamic Therapy Applications. *Eur. J. Inorg. Chem.* **2020**, *2020* (34), 3242-3248.
49. Dickerson, M.; Howerton, B.; Bae, Y.; C. Glazer, E., Light-Sensitive Ruthenium Complex-loaded Cross-linked Polymeric Nanoassemblies for the Treatment of Cancer. *J. Mater. Chem. B* **2016,** *4* (3), 394-408.
50. Appold, M.; Mari, C.; Lederle, C.; Elbert, J.; Schmidt, C.; Ott, I.; Stühn, B.; Gasser, G.; Gallei, M., Multi-Stimuli Responsive Block Copolymers as a smart Release Platform for a Polypyridyl Ruthenium Complex. *Polym. Chem.* **2017,** *8* (5), 890-900.
51. Chen, B.; Metera, K.; Sleiman, H. F., Biotin-Terminated Ruthenium Bipyridine Ring-Opening Metathesis Polymerization Copolymers: Synthesis and Self-Assembly with Streptavidin. *Macromolecules* **2005,** *38* (4), 1084-1090.
52. Sun, W.; Wen, Y.; Thiramanas, R.; Chen, M.; Han, J.; Gong, N.; Wagner, M.; Jiang, S.; Meijer, M. S.; Bonnet, S.; Butt, H.-J.; Mailänder, V.; Liang, X.-J.; Wu, S., Red-Light-Controlled Release of Drug–Ru Complex Conjugates from Metallopolymer Micelles for Phototherapy in Hypoxic Tumor Environments. *Adv. Funct. Mater.* **2018,** *28* (39), 1804227.
53. Ruggi, A.; Beekman, C.; Wasserberg, D.; Subramaniam, V.; Reinhoudt, D. N.; van Leeuwen, F. W. B.; Velders, A. H., Dendritic Ruthenium(II)-Based Dyes Tuneable for Diagnostic or Therapeutic Applications. *Chem. Eur. J.* **2011,** *17* (2), 464-467.
54. Shen, J.; Kim, H.-C.; Wolfram, J.; Mu, C.; Zhang, W.; Liu, H.; Xie, Y.; Mai, J.; Zhang, H.; Li, Z.; Guevara, M.; Mao, Z.-W.; Shen, H., A Liposome Encapsulated Ruthenium Polypyridine Complex as a Theranostic Platform for Triple-Negative Breast Cancer. *Nano Lett.* **2017,** *17* (5), 2913-2920.
55. Askes, S. H. C.; Bahreman, A.; Bonnet, S., Activation of a Photodissociative Ruthenium Complex by Triplet–Triplet Annihilation Upconversion in Liposomes. *Angew. Chem. Int. Ed.* **2014,** *53* (4), 1029-1033.
56. Karges, J.; Kuang, S.; Maschietto, F.; Blacque, O.; Ciofini, I.; Chao, H.; Gasser, G., Rationally designed ruthenium complexes for 1- and 2-photon photodynamic therapy. *Nat. Commun.* **2020,** *11* (1), 3262.
57. Li, J.; Wang, X.; Zhang, T.; Wang, C.; Huang, Z.; Luo, X.; Deng, Y., A Review on Phospholipids and their Main Applications in Drug Delivery Systems. *Asian J. Pharm. Sci.* **2015,** *10* (2), 81-98.
58. Feuvrie, C.; Maury, O.; Le Bozec, H.; Ledoux, I.; Morrall, J. P.; Dalton, G. T.; Samoc, M.; Humphrey, M. G., Nonlinear Optical and Two-Photon Absorption Properties of Octupolar Tris(bipyridyl)metal Complexes. *J. Phys. Chem. A* **2007,** *111* (37), 8980-8985.
59. Fang, J.; Nakamura, H.; Maeda, H., The EPR Effect: Unique Features of Tumor Blood Vessels for Drug Delivery, Factors involved, and Limitations and Augmentation of the Effect. *Adv. Drug Delivery Rev.* **2011,** *63* (3), 136-151.
60. Villemin, E.; Ong, Y. C.; Thomas, C. M.; Gasser, G., Polymer Encapsulation of Ruthenium Complexes for Biological and Medicinal Applications. *Nat. Rev. Chem.* **2019,** *3* (4), 261-282.
61. Maiti, S.; Paira, P., Biotin Conjugated Organic Molecules and Proteins for Cancer Therapy: A Review. *Eur. J. Med. Chem.* **2018,** *145*, 206-223.

62. Tripodo, G.; Mandracchia, D.; Collina, S.; Rui, M.; Rossi, D., New Perspectives in Cancer Therapy: The Biotin-Antitumor Molecule Conjugates. *Med. Chem.* **2014,** *8*, 1-4.
63. Karges, J.; Basu, U.; Blacque, O.; Chao, H.; Gasser, G., Polymeric Encapsulation of Novel Homoleptic Bis(dipyrrinato) Zinc(II) Complexes with Long Lifetimes for Applications as Photodynamic Therapy Photosensitisers. *Angew. Chem. Int. Ed.* **2019,** *58* (40), 14334-14340.
64. Karges, J.; Blacque, O.; Chao, H.; Gasser, G., Polymeric Bis(dipyrrinato) Zinc(II) Nanoparticles as Selective Imaging Probes for Lysosomes of Cancer Cells. *Inorg. Chem.* **2019,** *58* (18), 12422-12432.
65. Li, J.; Zeng, L.; Xiong, K.; Rees, T. W.; Jin, C.; Wu, W.; Chen, Y.; Ji, L.; Chao, H., A Biotinylated Ruthenium(ii) Photosensitizer for Tumor-Targeted Two-Photon Photodynamic Therapy. *Chem. Commun.* **2019,** *55* (73), 10972-10975.
66. Friedrich, J.; Seidel, C.; Ebner, R.; Kunz-Schughart, L. A., Spheroid-Based Drug Screen: Considerations and Practical Approach. *Nat. Protoc.* **2009,** *4* (3), 309-324.
67. Pluen, A.; Boucher, Y.; Ramanujan, S.; McKee, T. D.; Gohongi, T.; di Tomaso, E.; Brown, E. B.; Izumi, Y.; Campbell, R. B.; Berk, D. A.; Jain, R. K., Role of Tumor–Host Interactions in Interstitial Diffusion of Macromolecules: Cranial vs. Subcutaneous Tumors. *Proc. Natl. Acad. Sci.* **2001,** *98* (8), 4628-4633.
68. Szadvári, I.; Krizanova, O.; Babula, P., Athymic Nude Mice as an Experimental Model for Cancer Treatment. *Physiol. Res.* **2016,** *65*, 441-453.
69. Nakamaru, K., Solvent Effect on the Nonradiative Deactivation of the Excited State of Tris(2,2´-bipyridyl)ruthenium(II) Ion. *Bull. Chem. Soc. Jpn.* **1982,** *55* (5), 1639-1640.
70. Garcìa‐Fresnadillo, D.; Georgiadou, Y.; Orellana, G.; Braun, A. M.; Oliveros, E., Singlet‐Oxygen ($1\Delta g$) Production by Ruthenium (II) Complexes containing Polyazaheterocyclic Ligands in Methanol and in Water. *Helv. Chim. Acta* **1996,** *79* (4), 1222-1238.

TOC